International Journal of Thermal Sciences 98 (2015) 228–236

Contents lists available at ScienceDirect

International Journal of Thermal Sciences

journal homepage: www.elsevier.com/locate/ijts

Estimation of state variables in the hyperthermia therapy of cancer with heating imposed by radiofrequency electromagnetic waves

Leonardo Antonio Bermeo Varon [a], Helcio Rangel Barreto Orlande [a, *], Guillermo Enrique Eliçabe [b]

[a] Federal University of Rio de Janeiro – UFRJ, Department of Mechanical Engineering, PEM/COPPE, Caixa Postal 68503, Rio de Janeiro, RJ, 21941-972, Brazil
[b] University of Mar del Plata, Institute of Materials Science and Technology – INTEMA (CONICET), J.B. Justo 4302, 7600 Mar del Plata, Argentina

ARTICLE INFO

Article history:
Received 21 November 2014
Received in revised form
15 June 2015
Accepted 27 June 2015
Available online xxx

Keywords:
Inverse problem
Hyperthermia
Radiofrequency
Nanoparticles
Particle filter
SIR

ABSTRACT

One of the major difficulties in any cancer treatment is to kill the cells of the tumor without affecting healthy cells. Recently, with the advancement of nanotechnology, the localized hyperthermia treatment of cancer has again gained interest from the scientific community. In this technique, the application of electromagnetic waves, possibly even over the surface of the patient's body, causes temperature increases in the tissues. By concentrating nanoparticles in the tumorous tissues, cell damages can be inflicted mostly to the region of interest. This paper deals with numerical simulations under uncertainties of the treatment of cancer based on hyperthermia induced by radiofrequency electromagnetic waves, where the tumor is supposed to be loaded with nanoparticles. The focus of the paper is on the solution of the inverse problem dealing with the estimation of state variables, like the temperature distribution in the tissues. The state estimation problem is solved with the Particle Filter, by utilizing the Sampling Importance Resampling (SIR) algorithm. An excellent agreement between estimated and exact temperatures is obtained, which may help medical doctors in the future to prescribe treatment protocols and also opens the possibility of devising control strategies for the hyperthermia treatment of cancer.

1. Introduction

Hyperthermia is a cancer treatment where the tumor tissues are brought to temperatures sufficiently high to kill their cells (in this case usually denoted as thermoablation) or to make them more susceptible to the effects of radiation or chemotherapeutic drugs. Studies have indicated that hyperthermia can damage cells at temperatures of 40–45 °C, particularly because malignant tumors have low levels of oxygen, nutrients and pH [1–9]. Hyperthermia therapy can be classified as local, regional and whole body. These therapies can be invasive or non-invasive, and are carried out by utilizing electromagnetic waves as the heating mechanism, majorly in the ranges of radiofrequency [10–21] and near-infrared [22–28].

Hyperthermia induced by Radiofrequency (RF) is a treatment for partial or total elimination of cancer through the heating imposed by electromagnetic waves in frequencies ranging from 3 kHz to 300 GHz. In some cases, it is also used as an adjuvant therapy together with radiotherapy or chemotherapy, in order to increase their efficacies [4,29,30]. Nowadays, the combination of RF induced hyperthermia with tissues loaded with nanoparticles has been widely studied. In this kind of therapy, nanoparticles introduced into the cancer cells increase the absorptivity at the wavelength of interest, so that the temperatures in the tumor tissues increase at higher rates than in the healthy tissues (without nanoparticles), thus damaging the tumor only [5].

For the study of RF induced hyperthermia, Maxwell's equations with frequency dependence [31] are used together with the bioheat transfer equation [32]. The solution of the mathematical formulation for such physical problem requires the knowledge of several physical properties and other input parameters, which are seldom known and, in general, exhibit large variability from individual to individual, or even for the same individual under different physiological conditions. Such parameters would need to be indirectly estimated via measurements of other variables in the model, as an inverse problem solution [17]. Therefore, with such input parameters, which contain uncertainties, the numerical simulation of the bioheat transfer problem associated with the hyperthermia treatment of cancer shall not be performed in deterministic form. For

* Corresponding author.
E-mail addresses: lebermeo@ufrj.br (L.A. Bermeo Varon), helcio@mecanica.coppe.ufrj.br (H.R. Barreto Orlande), gelicabe@gmail.com (G.E. Eliçabe).

http://dx.doi.org/10.1016/j.ijthermalsci.2015.06.022
1290-0729/

Nomenclature

C	specific heat
$\mathbf{E}$	electric field strength
$\mathbf{H}$	intensity of the magnetic field
h_f	heat transfer coefficient
k	thermal conductivity
L_x, L_y	domain lengths in the x and y directions, respectively
n	number of nanoparticles
N	number of particles for the particle filter
Q	volumetric heat source
s	interface between the tumor and the surrounding tissue
T	temperature
T_f	temperature of the surrounding medium
t	time
w	weights
$\mathbf{x}$	state vector
x,y	Cartesian coordinates
$\mathbf{z}$	vector of measurements

Greeks

ε	permittivity
$\pi(a\|b)$	conditional probability of a when b is given
ρ	density
Ω'	surface of the domain
$\Omega_1^{'}$, $\Omega_2^{'}$	boundary patches with electrodes set to voltages U and ground, respectively
ω_b	blood perfusion rate
φ	electric potential
σ	electric conductivity
χ	susceptibility of the magnetic nanoparticles

Superscripts

i	particle index
meas	measurements

Subscripts

1	health tissue
2	tumor
b	blood
m	metabolism
e	electrical

example, if temperature measurements are available, the simulation of the stochastic bioheat transfer problem can be performed as a state estimation problem [33]. This is the approach considered in this work, where the RF induced hyperthermia is treated as an inverse problem of state estimation based on stochastic evolution and observation models, with minimally invasive temperature measurements. The present work aims at the better prediction of the temperature field in tumor and healthy tissues; the ultimate objectives are to improve this cancer treatment and reduce damages to the healthy cells, which may eventually help medical doctors with the planning of individual treatment protocols and also opens the possibility of devising real-time control strategies. For the case examined here, nanoparticles of iron oxide (Fe_3O_4) were considered to be loaded in the tumor region. A two-dimensional domain was used in the analysis [10,34,35] and the forward problem, involving Maxwell's and Pennes' equations, was solved with Comsol Multiphysics® 4.4. The Sampling Importance Resampling (SIR) algorithm [33] used for the solution of the inverse problem, which is coupled to the forward problem solution, was coded in Matlab®. The inverse problem was solved with simulated temperature measurements.

2. Physical problem and mathematical formulation

The physical problem examined in this work involves a rectangular domain, consisting of a circular tumor (Ω_2) located at the center of the rectangle and surrounded by healthy tissue (Ω_1), as illustrated by Fig. 1. Heating is imposed by the radiofrequency through the electrodes $\Omega_1^{'}$ and $\Omega_2^{'}$, which are maintained at the voltages U and zero, respectively. The remaining surfaces are electrically insulated. Heat generated by radiofrequency electromagnetic waves inside the domain is propagated by conduction and blood perfusion. The lateral surfaces of the domain are supposed thermally insulated, while the top and bottom surfaces exchange heat by convection with a surrounding medium. The region is supposed to be initially at the steady state temperature of the problem, when the source term (imposed by the radiofrequency external excitation) is null. This physical problem is similar to those considered in Refs. [10,14,34].

The electric potential, $\varphi(x,y)$, within the domain can be obtained by solving the following Laplace's equation [12,36–40]:

$$\nabla\cdot[\varepsilon(x,y)\nabla\varphi(x,y)] = 0 \quad x,y \in \Omega_1 \cup \Omega_2 \tag{1}$$

where x,y are the Cartesian coordinates with origin at the center of the tumor, ε is the permittivity that varies spatially depending on the tissue and tumor regions.

The interface, s, between the tumor and normal tissues is assumed to have perfect electric contact, that is,

$$\begin{cases} \varphi_1 = \varphi_2 \\ \varepsilon_1 \dfrac{\partial\varphi_1}{\partial\mathbf{n}} = \varepsilon_2 \dfrac{\partial\varphi_2}{\partial\mathbf{n}} \quad \text{at the interface } s \end{cases} \tag{2}$$

The boundary conditions for Eq. (1) are given by

$$\varphi = U \quad \text{at } x,y \in \Omega_1^{'} \tag{3}$$

$$\varphi = 0 \quad \text{at } x,y \in \Omega_2^{'} \tag{4}$$

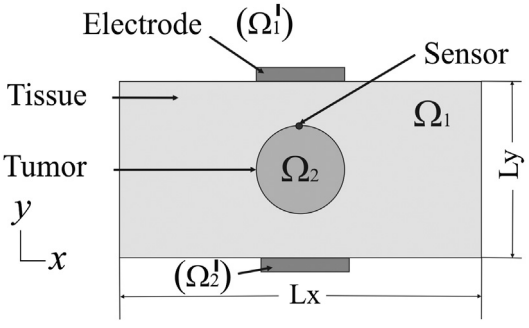

Fig. 1. Rf hyperthermia system.

$$\frac{\partial \varphi}{\partial \mathbf{n}} = 0 \quad \text{at } x,\ y \in \Omega' \quad \text{except at } \Omega_1',\ \ \Omega_2' \tag{5}$$

where Ω' denotes the surface of the domain, with boundary patches Ω_1' and Ω_2' in perfect contact with the electrodes, where the voltages U and zero are respectively imposed.

After the potential $\varphi(x,y)$ is computed from the solution of the problem given by Equations (1)–(5), the electric field strength E and the intensity of the magnetic field $\mathbf{H}$ can be obtained respectively from:

$$\mathbf{E}(x,y) = -\nabla\varphi(x,y) \tag{6}$$

$$|\mathbf{H}(x,y)| = \frac{1}{1+N(\chi)}\frac{|\mathbf{E}(x,y)|}{\mu_o \pi f R} \tag{7}$$

where $N(\chi) = 1/3$ is the demagnetizing factor of the composite tissue [12,41], χ is the susceptibility of the magnetic nanoparticles that can be described in terms of complex susceptibility $\chi = \chi' + i\chi''$ [12,42,43], μ_o is the dielectric constant permeability of the free space ($\mu_o = 4\pi x\ 10^{-7}$T m A^{-1}), f is the electromagnetic frequency and R is the radius of magnetic induction loop.

The mathematical formulation for heat transfer is described in this work by Pennes' Bioheat Transfer Equation [32], which is given by

$$\rho C\frac{\partial T(x,y,t)}{\partial t} = \nabla\cdot[k\nabla T(x,y,t)] - \omega_b(x,y)\rho_b C_b T(x,y,t) + Q(x,y) \quad x,y \in \Omega_1 \cup \Omega_2,\quad t > 0 \tag{8}$$

where ρ is the tissue density, C is the tissue specific heat, T is the temperature, k is the tissue thermal conductivity, ω_b is the blood perfusion rate, ρ_b is the blood density, C_b is the blood specific heat and Q is the volumetric heat source term resulting from the perfused blood, the tissue metabolism and the external electromagnetic excitation, that is,

$$Q = \omega_b(x,y)\rho_b C_b T_b(x,y) + Q_m(x,y) + Q_e(x,y) \tag{9}$$

where T_b is the blood temperature, Q_m is the metabolic heat source and Q_e is the heat source generated by the imposed electromagnetic fields, which depends on tissue, tumor and nanoparticles properties [12].

For the healthy tissue, which is assumed in this work to be free of nanoparticles, we have

$$Q_{e_1}(x,y) = \frac{\sigma_1|\mathbf{E}(x,y)|^2}{2} \text{ in } \Omega_1 \tag{10}$$

where σ_1 is the electric conductivity of the tissue.

In the tumor, the contribution for the electric heat source resulting from the presence of the magnetic nanoparticles is obtained from Refs. [12,21]:

$$Q_n = \mu_0 \pi f \chi'' |\mathbf{H}(x,y)|^2 \tag{11}$$

This quantity is added to the source term resulting from the electrical conduction through the tumor tissue, thus resulting in Refs. [12,41]:

$$Q_{e_2}(x,y) = (1-\theta)\frac{\sigma_2|\mathbf{E}(x,y)|^2}{2} + \theta\left(\frac{9}{16}\frac{\chi''}{\mu_o \pi f R^2}|\mathbf{E}(x,y)|^2\right) \text{ in } \Omega_2 \tag{12}$$

Here $\theta = n\pi r^2/A$ is the concentration of nanoparticles, that is, the total cross section of the nanoparticles divided by the area A of the tumor, while r is the mean radius of the supposedly spherical nanoparticles and n is the number of nanoparticles.

The electric conductivity of the tumor loaded with nanoparticles, σ_2, can be approximated by an arrangement in series, that is,

$$1/\sigma_2 = (1-\theta)\Big/\sigma_2' + \theta/\sigma_3 \tag{13}$$

where σ_2' and σ_3 are the electrical conductivities of the tumor tissue and of the nanoparticles, respectively. The permittivity of the tumor embedded with nanoparticles is approximated by that of the tumor. Such is the case because the volume concentration of particles is small and differences in this parameter for biological tissues and nanoparticles are not large [12].

The interface between the tumor and normal tissues is assumed to be in perfect thermal contact, that is,

$$\begin{cases} T_1 = T_2 \\ -k_1\dfrac{\partial T_1}{\partial \boldsymbol{n}} = -k_2\dfrac{\partial T_2}{\partial \boldsymbol{n}} \quad \text{at the interface } s \text{ for } t>0 \end{cases} \tag{14}$$

and the thermal boundary conditions at the surface of the region are given by:

$$\begin{cases} k_1\dfrac{\partial T_1}{\partial x} = 0 & \text{at } x = -\dfrac{L_x}{2} \text{ and } x = +\dfrac{L_x}{2}, -\dfrac{L_y}{2} < y < +\dfrac{L_y}{2},\ t>0 \\ -k_1\dfrac{\partial T_1}{\partial y} + h_f T = h_f T_f & \text{at } y = -\dfrac{L_y}{2}, -\dfrac{L_x}{2} < x < +\dfrac{L_x}{2},\ t>0 \\ k_1\dfrac{\partial T_1}{\partial y} + h_f T = h_f T_f & \text{at } y = +\dfrac{L_y}{2}, -\dfrac{L_x}{2} < x < +\dfrac{L_x}{2},\ t>0 \end{cases} \tag{15}$$

where h_f is the heat transfer coefficient, T_f is the temperature of the surrounding medium and L_x and L_y are the domain lengths in the x and y directions, respectively.

The initial condition for the problem is given by

$$T(x,y,t) = T_0(x,y) \quad \text{at } t = 0,\ \text{in } x,y \in \Omega_1 \cup \Omega_2 \tag{16}$$

where $T_0(x,y)$ is the solution of the steady state version of the problem given by Equations (8)–(15), for no heat generation from the external RF excitation, that is, $Q_e = 0$, and $T_f = 25$ °C, $h_f = 10$ W m^{-2} K^{-1}.

The bioheat transfer problem given by Equations (8) and (14) to (16), with source term (see Equations (9)–(13)) obtained from the solution of the electric potential problem given by Equations (1)–(5), is a direct (forward) problem when all the physical properties, geometry, initial and boundary conditions are known. Note that, for the solution of the forward problem, the electric potential can be computed independently of the temperature field in the medium; but the bioheat transfer problem is coupled to the electric potential problem through the source term imposed by the RF excitation.

3. State estimation problem

In this work, we solve the inverse problem of estimating the transient temperature field in the medium, by using temperature measurements obtained at one single location within the domain. Measurements and the solution of the forward problem are considered to contain uncertainties and the inverse problem is solved as a state estimation problem, as described below.

For the definition of the state estimation problem, consider a model for the evolution of the vector $\mathbf{x}$ in the following form [44].

$$\mathbf{x}_k = \mathbf{f}_k(\mathbf{x}_{k-1}, \mathbf{v}_{k-1}) \tag{17}$$

where the subscript $k = 1, 2,\ldots$, denotes a time instant t_k in a dynamic problem. The vector $\mathbf{x} \in R^{n_x}$ is called the state vector and contains the variables to be dynamically estimated. This vector advances in accordance with the state evolution model given by Equation (17), where $\mathbf{f}_k$ is a general function of the state variables $\mathbf{x}$ and of the state noise vector $\mathbf{v} \in R^{n_v}$.

Consider also that measurements $\mathbf{z}_k^{meas} \in R^D$ are available at t_k, $k = 1, 2, \ldots$. An observation model, which takes into account the physics of the measurement process and relates the measurements to the state variables $\mathbf{x}_k$ is given by:

$$\mathbf{z}_k = \mathbf{h}_k(\mathbf{x}_k, \mathbf{n}_k) \tag{18}$$

where $\mathbf{n} \in R^D$ is the measurement noise.

The state estimation problem aims at obtaining information about $\mathbf{x}_k$ based on the state evolution and measurement models, given by Equations (17) and (18), respectively, and on the measurements $\mathbf{z}_{1:k}^{meas} = [\mathbf{z}_1^{meas}, \mathbf{z}_2^{meas}, \ldots, \mathbf{z}_k^{meas}]$ [44–46]. The evolution-observation models are based on the following assumptions [45,46]:

i. The sequence $\mathbf{x}_k$ for $k = 1, 2, \ldots$, is a Markovian process, that is,

$$\pi(\mathbf{x}_k|\mathbf{x}_0, \mathbf{x}_1, \ldots, \mathbf{x}_{k-1}) = \pi(\mathbf{x}_k|\mathrm{x}_{k-1}) \tag{19}$$

ii. The sequence $\mathbf{z}_k$ for $k = 1,2, \ldots$, is a Markovian process with respect to the history of $\mathbf{x}_k$, that is,

$$\pi(\mathbf{z}_k|\mathbf{x}_0, \mathbf{x}_1, \ldots, \mathbf{x}_k) = \pi(\mathbf{z}_k|\mathbf{x}_k) \tag{20}$$

iii. The sequence $\mathbf{x}_k$ depends on the past observations only through its own history, that is,

$$\pi(\mathbf{x}_k|\mathbf{x}_{k-1}, \mathbf{z}_{1:k-1}) = \pi(\mathbf{x}_k|\mathbf{x}_{k-1}) \tag{21}$$

For the evolution-observation model given by Equations (17) and (18), the noise vectors are also assumed to be mutually independent and independent of the initial state $\mathbf{x}_0$ [45].

In this paper, we solve the so-called filtering problem, which aims at obtaining the posterior probability $\pi(\mathbf{x}_k|\mathbf{z}_{1:k})$. By assuming that $\pi(\mathbf{x}_0|\mathbf{z}_0) = \pi(\mathbf{x}_0)$ is available at time t_0, $\pi(\mathbf{x}_k|\mathbf{z}_{1:k})$ is obtained with Bayesian filters in two sequential steps, namely: prediction and update [44–46]. The state evolution model is used to advance the vector of state variables from time t_{k-1} to time t_k in the prediction step, thus obtaining a prior distribution $\pi(\mathbf{x}_k)$ for the state variables at time t_k. The information provided by the measurements is then adjoined to this prior distribution in the update step through Bayes' theorem, by using the likelihood function $\pi(\mathbf{z}_k|\mathbf{x}_k)$ [44,45].

The Particle Filter method is used in this work. It is a Monte Carlo technique for the solution of state estimation problems, where the required posterior density function is represented by a set of random samples (particles) with associated weights; the statistics of the posterior distribution is then computed based on these samples and weights. Differently from the Kalman filter, the application of the Particle Filter is not limited to linear and Gaussian models. The particle filter algorithms generally make use of an importance density, which is a density proposed to represent another one that cannot be computed exactly, that is, the sought posterior density in the present case. Then, samples are drawn from the importance density instead of the actual density [45,47,48].

Let $\mathbf{x}_{0:k}^i$ be the particles with associated weights w_k^i, $i = 1, \ldots, N$ and $\mathbf{x}_{0:k} = \mathbf{x}_j$, $j = 0,1,\ldots,k$ be the set of all state variables up to t_k, where N is the number of particles. The weights are normalized so that $\sum_{i=1}^N w_k^i = 1$. Then, the posterior density at t_k can be discretely approximated by Refs. [45,47,48]:

$$\pi(\mathbf{x}_{0:k}|\mathbf{z}_{1:k}) \approx \sum_{i=1}^{N} w_k^i \delta\left(\mathbf{x}_{0:k} - \mathbf{x}_{0:k}^i\right) \tag{22}$$

where $\delta(.)$ is the Dirac δ function. Similarly, its marginal distribution, which is of interest for the filtering problem, can be approximated by

$$\pi(\mathbf{x}_k|\mathbf{z}_{1:k}) \approx \sum_{i=1}^{N} w_k^i \delta\left(\mathbf{x}_k - \mathbf{x}_k^i\right) \tag{23}$$

with weights computed from

$$w_k^i \propto w_{k-1}^i \frac{\pi\left(\mathbf{z}_k|\mathbf{x}_k^i\right)\pi\left(\mathbf{x}_k^i|\mathbf{x}_{k-1}^i\right)}{q\left(\mathbf{x}_k^i\middle|\mathbf{x}_{k-1}^i, \mathbf{z}_k\right)} \tag{24}$$

where the importance density $q(\mathbf{x}_k^i|\mathbf{x}_{k-1}^i, \mathbf{z}_{1:k})$ was assumed to be given by $q(\mathbf{x}_k^i|\mathbf{x}_{k-1}^i, \mathbf{z}_k)$, that is, it depends only on $\mathbf{x}_{k-1}^i$ and $\mathbf{z}_k$, instead of the whole histories of each particle and of the measurements [45,47,48]. Due to practical difficulties, a suboptimal importance density is used in Equation (24), which is then given by the transitional prior, that is, $q(\mathbf{x}_k^i|\mathbf{x}_{k-1}^i, \mathbf{z}_k) = \pi(\mathbf{x}_k^i|\mathbf{x}_{k-1}^i)$ [48]. Hence, Equation (24) reduces to:

$$w_k^i \propto w_{k-1}^i \pi\left(\mathbf{z}_k|\mathbf{x}_k^i\right) \tag{25}$$

The sequential application of the particle filter might result in the degeneracy phenomenon, where after a few states all but very few particles have negligible weight [44,45,48]. This problem can be overcome with a resampling step in the application of the particle filter, which involves a mapping of the random measure $\{\mathbf{x}_k^i, w_k^i\}$ into $\{\mathbf{x}_k^{i*}, N^{-1}\}$ with uniform weights. Resampling can be performed if the number of effective particles (particles with large weights) falls below a certain threshold number, or at every instant t_k, such as in the Sampling Importance Resampling (SIR) algorithm described in Refs. [44,48]. The SIR algorithm used in this work is summarized in Table 1, as applied to the system evolution from t_{k-1} to t_k [44,48]. It should be noted in Table 1 that the weights in the SIR algorithm are given directly by the likelihood function $\pi(\mathbf{z}_k|\mathbf{x}_k^i)$. Such is the case because in this algorithm the resampling step is applied at each time instant and then the weights w_{k-1}^i are uniform and given by N^{-1}(see Equation (25)).

By assuming that the measurement errors are additive, uncorrelated, Gaussian random variables with zero means and known constant standard deviation, ν, and independent of the state variables, the likelihood function for each particle $\mathbf{x}_k^i$ can be expressed as [44,45,48]:

Table 1
Sampling Importance Resampling algorithm [44,48].

Step 1
For $i = 1,\ldots,N$ draw new particles $\mathbf{x}_k^i$ from the prior density $\pi(\mathbf{x}_k\|\mathbf{x}_{k-1}^i)$ and then use the likelihood density to calculate the corresponding weights $w_k^i = \pi(\mathbf{z}_k\|\mathbf{x}_k^i)$.
Step 2
Calculate the total weight $T_w = \sum_{i=1}^N w_k^i$ and then normalize the particle weights, that is, for $i = 1,\ldots,N$ let $w_k^i = T_w^{-1} w_k^i$
Step 3
Resample the particles as follows: Construct the cumulative sum of weights (CSW) by computing $c_i = c_{i-1} + w_k^i$ for $i = 1,\ldots,N$, with $c_0 = 0$. Let $i = 1$ and draw a starting point u_1 from the uniform distribution $U[0, N^{-1}]$ For $j = 1,\ldots,N$ Move along the CSW by making $u_j = u_1 + N^{-1}(j-1)$ While $u_j > c_i$ make $i = i+1$. Assign sample $\mathbf{x}_k^j = \mathbf{x}_k^i$ Assign weight $w_k^j = N^{-1}$

$$\pi\left(\mathbf{z}_k\middle|\mathbf{x}_k^i\right) = (2\pi)^{-D/2}\nu^{-D}\exp\left\{-\frac{1}{2}\frac{\left[\mathbf{z}_k^{meas} - \mathbf{z}_k\left(\mathbf{x}_k^i\right)\right]^T\left[\mathbf{z}_k^{meas} - \mathbf{z}_k\left(\mathbf{x}_k^i\right)\right]}{\nu^2}\right\} \quad (26)$$

where $\mathbf{z}_k(\mathbf{x}_k^i)$ is obtained from the observation model given by Equation (18) and D is the number of measurements.

4. Results and discussions

For all cases examined below, a rectangular two dimensional domain with dimensions $L_x = 80$ mm and $L_y = 40$ mm was considered, while the tumor was assumed as a circle of radius 10 mm located at the center of the rectangular domain. The lengths of both electrodes are 20 mm and they are centered at the top and bottom surfaces of the domain. The healthy tissue is assumed to be muscle. Thermophysical properties of blood, healthy and tumorous tissues are given by: $k_1 = k_2 = 0.5$ W m^{-1} K^{-1}, $C_b = C_1 = C_2 = 4200$ J kg^{-1} K^{-1}, $\rho_b = \rho_1 = \rho_2 = 1000$ kgm^{-3}, $\omega_{b1} = 0.0005$ s^{-1}, $\omega_{b2} = 0.002$ s^{-1}, $T_b = 37$ °C, $Q_{m1} = 4200$ W m^{-3} and $Q_{m2} = 42{,}000$ W m^{-3}. For the convective boundary conditions we assume $T_f = 20$ °C and $h_f = 45$ W m^{-2} K^{-1} [10]. For the iron oxide nanoparticles (Fe_3O_4), the following properties have been considered: $k_3 = 40$ W m^{-1} K^{-1}, $C_3 = 4000$ J kg^{-1} K^{-1}, $\rho_3 = 5180$ kg m^{-3} [12]. The electrical properties were considered as dependent of the frequency of the imposed electromagnetic wave, namely: (i) for $f = 1$ MHz, we have $\sigma_1 = 0.50268$ S/m and $\varepsilon_1 = 1836.4$; (ii) for $f = 10$ MHz, we have $\sigma_1 = 0.61683$ S/m and $\varepsilon_1 = 170.73$ [49]. The properties for the tumor were taken as $\sigma_2' = 1.2\sigma_1$ and $\varepsilon_2' = \varepsilon_2 = 1.2\varepsilon_1$, while for the nanoparticles the electric conductivity was assumed as $\sigma_3 = 25{,}000$ S/m [10]. For all cases examined below, the number of nanoparticles was $n = 10^8$, with radius $r = 10^{-8}$ m and $\chi = 18$, while the voltage at the electrode at the top boundary was $U = 10$ V. The nanoparticles were assumed to be located only within the tumor. The initial condition for the bioheat transfer problem, which is the solution of the steady state version of the problem given by Equations (8)–(14), is presented by Fig. 2.

Before examining the solution of the state estimation problem, we present the solution of the direct (forward) problem obtained with Comsol Multiphysics® 4.4 and verified against the results presented by Ref. [14]. Fig. 3a,b shows the temperature distributions in the region (solution of the direct problem) at time $t = 900$ s, for $f = 1$ MHz and $f = 10$ MHz, respectively. The analyses of these figures reveal that the use of nanoparticles in the tumor resulted in substantial temperature increases that are, in practical terms, limited to the tumor region. The maximum temperature in the region for $f = 1$ MHz was 44.8 °C, while for $f = 10$ MHz it was 40.8 °C. Such maximum temperatures took place at the center of the tumor. Differences observed in the temperature distributions for the two frequencies examined are due to the frequency dependence of the electrical properties. The electrical volumetric heat source term given by Equations (10) and (11), for $f = 1$ MHz and $f = 10$ MHz, are shown by Fig. 4a,b, respectively. One can notice in these figures that the electrical heat source attains its maximum values near the electrodes, and that they are larger for $f = 10$ MHz. The electrical volumetric heat source is more concentrated in the tumor region for $f = 1$ MHz, thus resulting in the larger temperatures in this region than for $f = 10$ MHz (see also Fig. 3a,b). Anyhow, for both cases the temperatures inside the tumor rise to values that are appropriate for the hyperthermia treatment [1–9].

For the solution of the state estimation problem, temperature measurements of one single sensor were assumed available for the inverse analysis, located at the position {$x = 0$ mm, $y = 10$ mm}. The measurements were generated from the solution of the direct problem with the parameters specified above. In order to avoid an inverse crime [45], the simulated measurements were generated on a grid with 2533 elements, while the inverse problem solution was obtained on a grid with 1591 elements. Uncorrelated Gaussian errors with zero mean and a standard deviation of 1 °C were then added to the solution of the direct problem. The simulated measurements were supposed available every 10 s.

The evolution model for the electrical volumetric heat source was taken in the form of a random walk, that is, for each particle i,

$$Q_{e,k}^i(x,y) = Q_{e,k-1}^i(x,y) + \xi_k^i(x,y) \quad (27)$$

where $\xi_k^i(x,y)$ is a Gaussian random variable with zero mean and a standard deviation of 10% of the deterministic solution of the electrical problem (see Fig. 4a,b). The subscript k in Equation (27) does not represent a time evolution of $Q_e(x,y)$, but the fact that it is treated as state variable for the application of the particle filter that aims at the estimation of the electric heat source and of the transient temperature field, at each position (x,y) of each finite-element used for the numerical solution of the coupled electric and bioheat transfer problem. The particles $Q_{e,0}^i(x,y)$ at each position (x,y) were initially sampled from Gaussian distributions with means obtained from the deterministic solution of the electric problem (see Fig. 4a,b) and with standard deviations of 10% of these means.

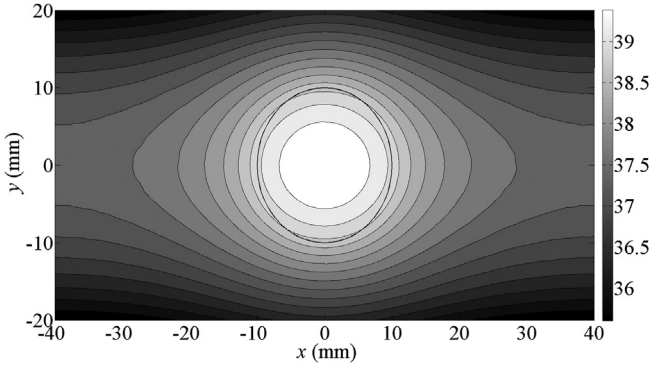

Fig. 2. Initial temperature.

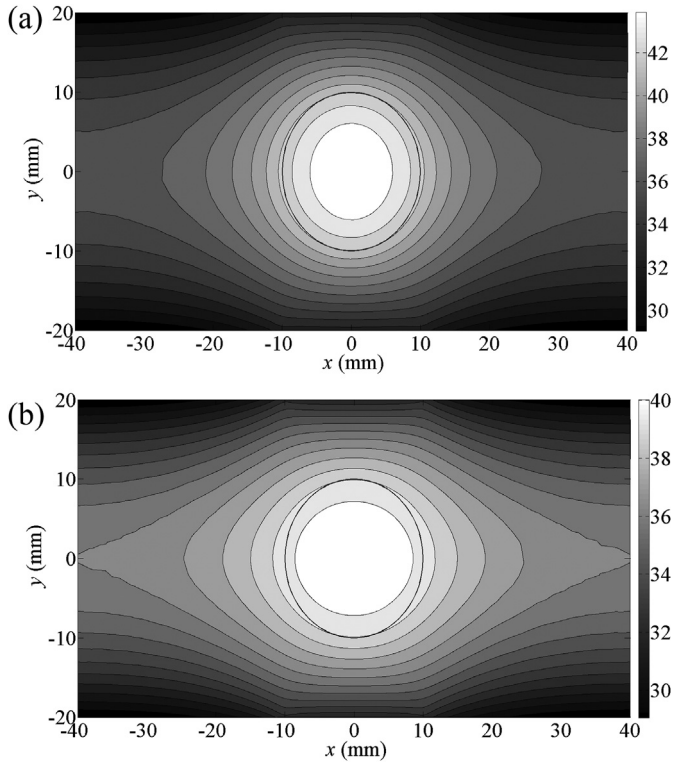

Fig. 3. Temperature distribution in the region at $t = 900$ s for: (a) $f = 1$ MHz and (b) $f = 10$ MHz.

The numerical discretization of the bioheat transfer problem given by Equations (8)–(16) constitutes the evolution model for the transient temperature field in the medium. In order to cope with uncertainties in such evolution model, e.g., in the thermophysical properties, a Gaussian uncorrelated noise with zero mean and a standard deviation of 1 °C was added to the solution of the bioheat transfer problem, which is solved with each sample of the Gaussian distribution of the electrical heat source term (see Equation (27)).

Fig. 5a–c presents the solution of the state estimation problem at the positions $\{x = 0, y = 10$ mm$\}$, $\{x = 10$ mm, $y = 0\}$ and $\{x = -40$ mm, $y = 20$ mm$\}$, respectively, for $f = 1$ MHz and 100 particles. We note in Fig. 5a that the estimated temperatures (means of the marginal posterior distributions) are in much better agreement with the exact ones than the measurements themselves are. Furthermore, Fig. 5b,c shows that the exact temperatures can be quite accurately estimated even at positions where no measurements are available. Such a fact becomes also evident from the analysis of Fig. 6, which presents the estimated temperature field at time $t = 900$ s and the estimated volumetric heat source (see also Figs. 3a and 4a). The maximum estimated temperature in the region at $t = 900$ s was 44.9 °C, which is in excellent agreement with the exact value of 44.8 °C.

Despite the fact that quite accurate estimates could be obtained for the solution of the inverse problem for $f = 1$ MHz with only 100 particles, the results can be further improved if the number of particles is increased. The results obtained with 500 particles for $f = 1$ MHz at the positions $\{x = 0, y = 10$ mm$\}$, $\{x = 10$ mm, $y = 0\}$ and $\{x = -40$ mm, $y = 20$ mm$\}$ are presented in Fig. 7a–c, respectively. A comparison of Figs. 5 and 7 clearly reveals that the agreement between estimated and exact temperatures improve, as well as the estimated confidence intervals become smoother, as the number of particles used in the particle filter algorithm was increased. The temperature distribution at $t = 900$ s estimated with 500 particles is shown by Fig. 8a. Indeed, the temperature distribution in the region also becomes smoother and in better agreement the exact one (see also Fig. 3a) when the number of particles was increased from 100 to 500. Such was also the case for the estimation of the electric volumetric heat source term (see Fig. 4a and 8b).

The computational time for the inverse problem solution with 100 particles and 500 particles was of 6.3 h and 31.5 h, respectively, on an Intel(R) Xeon E56445@2.40GHz dual processor with 32 GB of RAM memory.

We now consider a case where the electromagnetic waves are imposed with frequency $f = 10$ MHz, which result in smaller temperature increases than the case with $f = 1$ MHz, as depicted by Fig. 3a,b. Based on the foregoing analysis, the results for $f = 10$ MHz are presented only for 500 particles. Fig. 9a–c presents the temperature variation at the locations $\{x = 0, y = 10$ mm$\}$, $\{x = 10$ mm, $y = 0\}$ and $\{x = -40$ mm, $y = 20$ mm$\}$, respectively. Such as for the case with $f = 1$ MHz, the SIR algorithm is capable of accurately predicting the temperature variations at the points where temperature measurements are available and where they are not available. The estimated temperature field at $t = 900$ s and the estimated electric volumetric heat source are respectively presented by Fig. 10a,b, respectively. A comparison of such two figures with Fig. 3b and 4b, respectively, reveal that the spatial variation of these quantities could be quite well recovered with the present inverse problem approach based on the particle filter method. The maximum predicted temperature in the region at $t = 900$ s was 41.0 °C, as compared to 40.8 °C for the deterministic simulation.

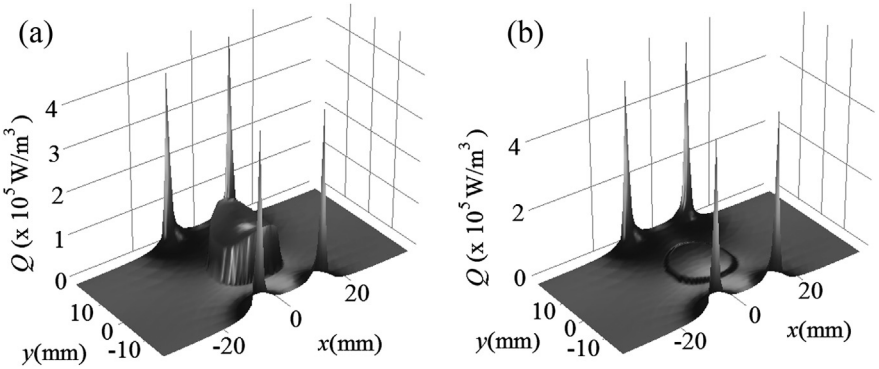

Fig. 4. Electrical volumetric heat source for: (a) $f = 1$ MHz and (b) $f = 10$ MHz.

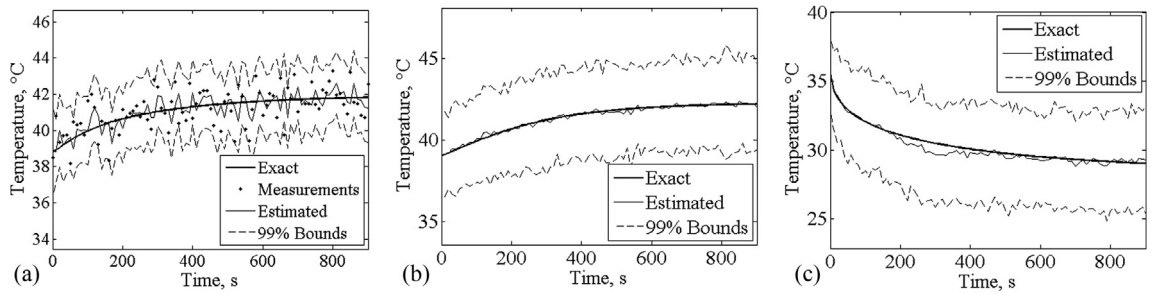

Fig. 5. Estimated transient variation of the temperature for $f = 1$ MHz and 100 particles at: (a) {$x = 0$, $y = 10$ mm}, (b) {$x = 10$ mm, $y = 0$} and (c) {$x = -40$ mm, $y = 20$ mm}.

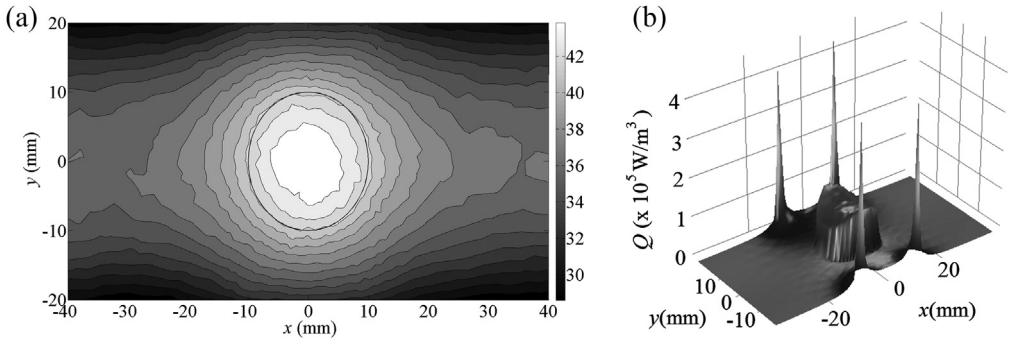

Fig. 6. (a) Estimated temperature field at time $t = 900$ s and (b) Estimated Electrical heat source for $f = 1$ MHz and 100 particles.

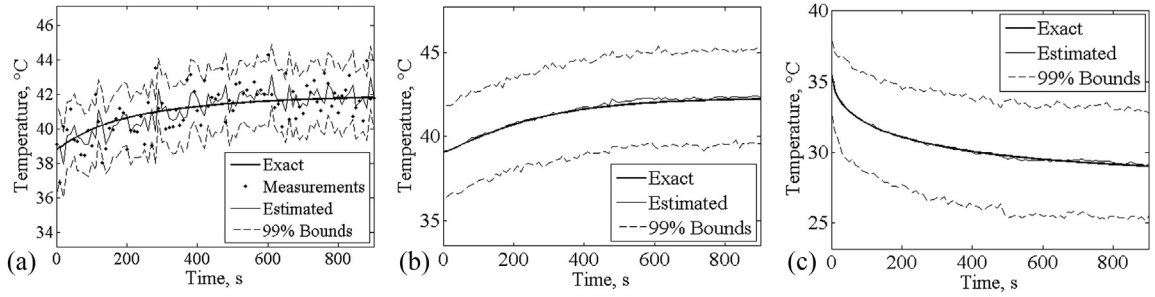

Fig. 7. Estimated transient variation of the temperature for $f = 1$ MHz and 500 particles at: (a) {$x = 0$, $y = 10$ mm}, (b) {$x = 10$ mm, $y = 0$} and (c) {$x = -40$ mm, $y = 20$ mm}.

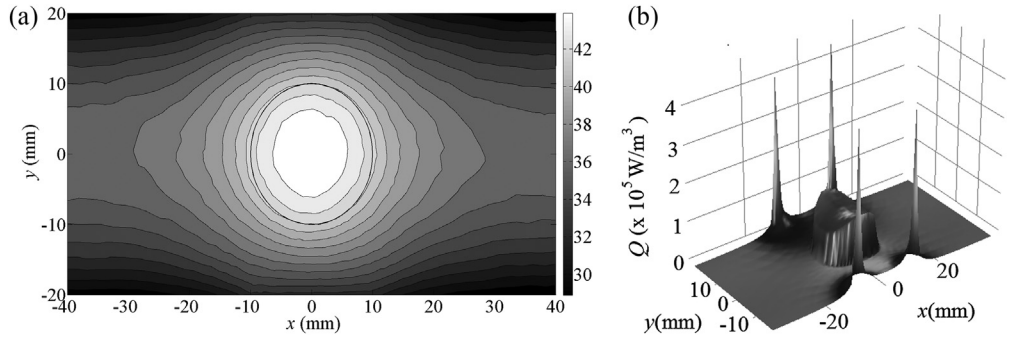

Fig. 8. (a) Estimated temperature field at time $t = 900$ s and (b) Estimated Electrical heat source; for $f = 1$ MHz and 500 particles.

5. Conclusions

The inverse problem of estimating the electric heat source and transient temperature fields in a two-dimensional region, for the coupled electric – bioheat transfer problem related to the hyperthermia treatment of cancer, is solved in this paper. The tumor region was supposed to be loaded with nanoparticles of iron oxide (Fe_3O_4) and transient temperature measurements are assumed available at one single location inside the domain. The inverse problem was solved as a state estimation problem, by using the Sampling Importance Resampling algorithm (SIR) of the particle filter method.

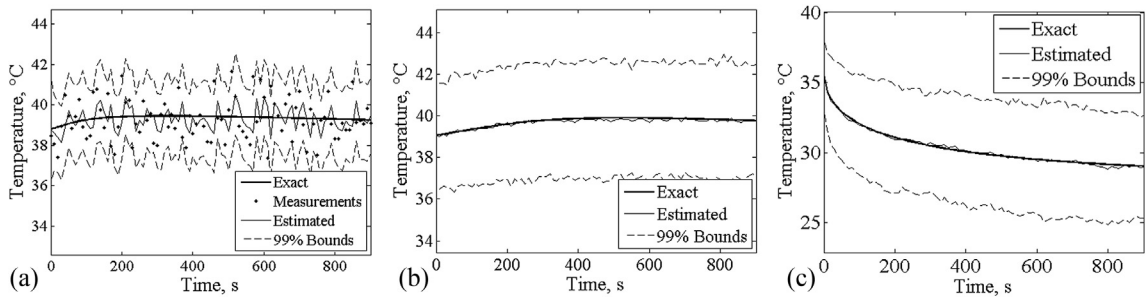

Fig. 9. Estimated transient variation of the temperature for $f = 10$ MHz and 500 particles at: (a) {$x = 0$, $y = 10$ mm}, (b) {$x = 10$ mm, $y = 0$} and (c) {$x = -40$ mm, $y = 20$ mm}.

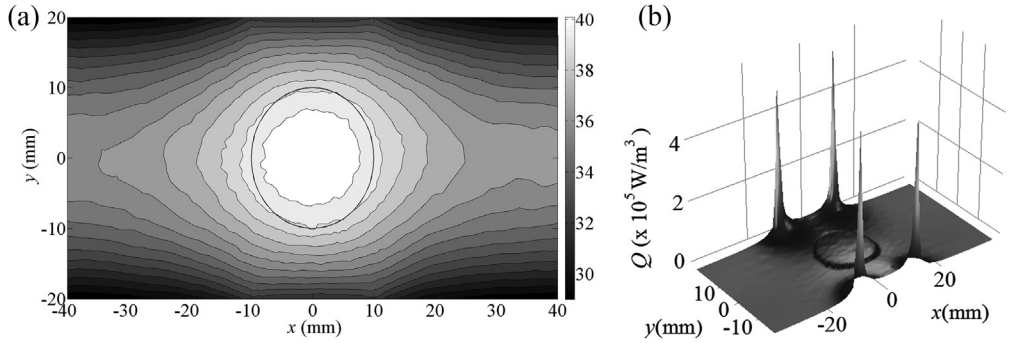

Fig. 10. (a) Estimated temperature field at time $t = 900$ s and (b) Estimated Electrical heat source; for $f = 10$ MHz and 500 particles.

Examples are given for estimations with two different frequencies of the imposed electric excitation in the Radiofrequency range. The effect of the number of particles in the inverse problem solution was also examined in the paper. The results obtained reveal that quite accurate estimations can be obtained for all cases examined, which involved large uncertainties in the evolution model and in the simulated measured data. As the number of particles was increased, the results became more accurate and smoother, but even with only 100 particles the estimated fields were in excellent agreement with the exact ones.

Acknowledgments

The financial support provided by FAPERJ, CAPES and CNPq, Brazilian agencies for the fostering of science, is greatly appreciated. The authors also acknowledge the support provided by the STIC AmSud project "I3PE – Inverse Problems in Physical Properties Estimation".

References

[1] S. Curto, Antenna Development for Radio Frequency Hyperthermia Applications [PhD Thesis], Dublin Institute of Tecnology, 2010.
[2] E.S. Glazer, Intracellular Hyperthermia Mediated by Nanoparticles in Radiofrequency Fields in the Treatment of Pancreatic Cancer [PhD Thesis], The University of Arizona, 2012.
[3] T. Niwa, Y. Takemura, T. Inoue, N. Aida, H. Kurihara, T. Hisa, Implant hyperthermia resonant circuit produces heat in response to MRI unit radiofrequency pulses, Br. J. Radiol. 81 (2008) 69–72.
[4] P. Wust, B. Hildebrandt, G. Sreenivasa, B. Rau, J. Gellermann, H. Riess, et al., Review hyperthermia in combined treatment of cancer, Lancet Oncol. 3 (2002) 487–497.
[5] S.H. Cho, S. Krisnan, Cancer Nanotechnology Principles and Applications in Radiation Oncology, CRC Press. Taylor & Francis, Boca Raton, FL, 2013.
[6] M. Dewhirst, L. Prosnitz, D. Thrall, D. Prescott, S. Clegg, C. Charles, et al., Hyperthermic treatment of malignant diseases: current status and a view toward the future, Semin. Oncol. 24 (1998) 616–625.
[7] C.A. Perez, T. Pajak, B. Emami, N.B. Hornback, L. Tupchong, P. Rubin, Randomized phase III study comparing irradiation and hyperthermia with irradiation alone in superficial measurable tumors. Final report by the Radiation Therapy Oncology Group, Am. J. Clin. Oncol. 14 (1991) 133–141.
[8] X. Yang, J. Du, Y. Liu, Advances in hyperthermia technology, in: Proc. 2005 IEEE Eng. Med. Biol. 27th Annu. Conf, vol. 7, 2005, pp. 6766–6769.
[9] J. Van Der Zee, D.G. Gonzalez, G.C. VanRhoon, J.D. van Dijk, W. van Putten, A.A. Hart, Comparison of radiotherapy alone with radiotherapy plus hyperthermia in locally advenced pelvic tumours: a prospective, randomised, multicentre trial, Lancet 355 (2000) 1119–1125.
[10] E. Majchrzak, M. Paruch, Numerical modelling of the cancer destruction during hyperthermia treatment, in: Comput. Methods Mech, 2011, pp. 1–6.
[11] E. Majchrzak, M. Paruch, Numerical Modelling of Tissue Heating by Means of the Electromagnetic Field, Sci. Res. Inst. Math. Comput. Sci, 2010, pp. 1–9.
[12] Y.-G. Lv, Z.-S. Deng, J. Liu, 3-D numerical study on the induced heating effects of embedded micro/nanoparticles on human body subject to external medical electromagnetic field, IEEE Trans. Nanobioscience 4 (2005) 284–294.
[13] A. Miaskowski, B. Sawicki, Magnetic fluid hyperthermia modeling based on phantom measurements and realistic breast model, IEEE Trans. Biomed. Eng. 60 (2013) 1806–1813.
[14] E. Majchrzak, M. Paruch, Numerical Modelling of Temperature Field in the Tissue with a Tumor Subject to the Action of Two External Electrode, Sci. Res. Inst. Math. Comput. Sci. 1 (2009) 1–8.
[15] L.A. Bermeo, H.R.B. Orlande, G. Elicabe, State estimation problem with particle filter for the radiofrequency hyperthermia therapy combined with nanoparticles, in: 15th Brazilian Congr. Therm. Sci. Eng., Belém, PA, Brazil, 2014, pp. 1–8.
[16] E. Kurgan, P. Gas, Treatment of tumors located in the human thigh using RF hyperthermia, Prz. Elektrotechniczny 87 (2011) 103–106.
[17] E. Kurgan, P. Gas, Estimation of temperature distribution inside tissues in external RF hyperthermia, Prz. Elektrotechniczny 86 (2010) 100–102.
[18] M. Jamil, E.Y.K. Ng, To optimize the efficacy of bioheat transfer in capacitive hyperthermia: a physical perspective, J. Therm. Biol. 38 (2013) 272–279, http://dx.doi.org/10.1016/j.jtherbio.2013.03.007.
[19] M. Jamil, E.Y.K. Ng, Ranking of parameters in bioheat transfer using Taguchi analysis, Int. J. Therm. Sci. 63 (2013) 15–21, http://dx.doi.org/10.1016/j.ijthermalsci.2012.07.002.
[20] M. Jamil, E.Y.K. Ng, Statistical modeling of electrode based thermal therapy with Taguchi based multiple regression, Int. J. Therm. Sci. 71 (2013) 283–291, http://dx.doi.org/10.1016/j.ijthermalsci.2013.03.014.
[21] E. Majchrzak, M. Paruch, Identification of electromagnetic field parameters assuring the cancer destruction during hyperthermia treatment, Inverse Probl. Sci. Eng. 19 (2011) 45–58.
[22] L.A. Dombrovsky, V. Timchenko, M. Jackson, G.H. Yeoh, A combined transient thermal model for laser hyperthermia of tumors with embedded Gold Nanoshells, Int. J. Heat Mass Transf. 54 (2011) 5459–5469.

[23] B. Lamien, H.R.B. Orlande, G. Elicabe, A.J. Maurente, State estimation problem in hyperthermia treatment of tumors loaded with nanoparticles, in: Proc. 15th Int. Heat Transf. Conf. IHTC-15, Kyoto, Japan, 2014, pp. 1–15.
[24] S. Eibner, R. Jaime, B. Lamien, R. Basto, H. Orlande, O. Fudym, Near infrared light heating of soft tissue phantoms containing nanoparticles, Therm. Eng. 13 (2014) 13–18.
[25] L.A. Dombrovsky, V. Timchenko, M. Jackson, Indirect heating strategy for laser induced hyperthermia: an advanced thermal model, Int. J. Heat Mass Transf. 55 (2012) 4688–4700.
[26] Y. Bayazitoglu, Nanoshell assisted cancer thermal therapy: numerical simulations, in: Proc. ASME 2009 2nd Micro/Nanoscale Heat Mass Transf. Int. Conf., Shanghai, China, 2009, pp. 1–8.
[27] X. Xu, A. Meade, Y. Bayazitoglu, Numerical investigation of nanoparticle-assisted laser-induced interstitial thermotherapy toward tumor and cancer treatments, Lasers Med. Sci. 26 (2011) 213–222.
[28] X. Xu, A. Meade, Y. Bayazitoglu, Feasibility of selective nanoparticle-assisted photothermal treatment for an embedded liver tumor, Lasers Med. Sci. (2012) 1–10.
[29] M.R. Horsman, J. Overgaard, Hyperthermia: a potent enhancer of radiotherapy, Clin. Oncol. R. Coll. Radiol. 19 (2007) 418–426.
[30] S. Jain, D.G. Hirst, J.M. O'Sullivan, Gold nanoparticles as novel agents for cancer therapy, Br. J. Radiol. 85 (2012) 101–113.
[31] J.C. Maxwell, A dynamical theory of the electromagnetic field, Philos. Trans. R. Soc. Lond. 155 (1865) 459–512.
[32] H.H. Pennes, Analysis of tissue and arterial blood temperatures in the resting human forearm, J. Appl. Physiol. 1 (1948) 93–124.
[33] N. Gordon, D. Salmond, A.F.M. Smith, Novel approach to nonlinear and non-Gaussian Bayesian state estimation, Proc. Inst. Elect. Eng. 140 (1993) 107–113.
[34] E. Majchrzak, G. Dziatkiewicz, M. Paruch, The modelling of heating a tissue subjected to external electromagnetic field, Acta Bioeng. Biomech./Wrocław Univ. Technol. 10 (2008) 29–37.
[35] E. Majchrzak, J. Drozdek, M. Paruch, Heating of Tissue by Means of the Electric Filed – Numerical Model Basing on the BEM, 2008, pp. 1–12.
[36] C.L. Antunes, T.R.O. Almeida, N. Raposeiro, Saline-enhanced RF ablation on a cholangiocarcinoma, Int. J. Comput. Math. Electr. Electron. Eng. 31 (2012) 1055–1066.
[37] E.J. Berjano, Theoretical modeling for radiofrequency ablation: state-of-the-art and challenges for the future, Biomed. Eng. Online 5 (2006) 24–39.
[38] D.K. Cheng, Fundamentals of Engineering Electromagnetics, Addison-Wesley Publishing Company, Inc, United State of America, 1993.
[39] G. Jiang, T. Qu, Z. Shang, X. Zhang, A circuit simulating method for heat transfer mechanism in human body, in: Annu. Int. Conf. IEEE Eng. Med. Biol. Soc., vol. 7, 2004, pp. 5274–5276.
[40] S. Tungjitkusolmun, E.J. Woo, H. Cao, V.R. Vorperian, J.G. Webster, J.Z. Tsai, Thermal-electrical finite element modelling for radio frequency cardiac ablation: effects of changes in myocardial properties, Med. Biol. Eng. Comput. (2000) 562–568.
[41] W. Andra, C.G. Ambly, R. Hergt, I. Hilger, W.A. Kaiser, Temperature distribution as function of time around a small spherical heat source of local magnetic hyperthermia, J. Magn. Magn. Mater. 194 (1999) 197–203.
[42] Q.A. Pankhurst, J. Connolly, S.K. Jones, J. Dobson, Applications of magnetic nanoparticles in biomedicine, J. Phys. D Appl. Phys. 36 (2003) R167–R181.
[43] R.E. Rosensweig, Heating magnetic fluid with alternating magnetic field, J. Magn. Magn. Mater. 252 (2002) 370–374.
[44] M.S. Arulampalam, S. Maskell, N. Gordon, T. Clapp, A tutorial on particle filters for online nonlinear/non-Gaussian Bayesian tracking, IEEE Trans. Signal Process 50 (2002) 174–188.
[45] J.P. Kaipio, E. Somersalo, Computational and Statistical Methods for Inverse Problems, Springer, Berlin, Heidelberg, 2004.
[46] P. Maybeck, Stochastic Models, Estimation, and Control, NY, USA, 1979.
[47] C. Andrieu, A. Doucet, Particle filtering for partially observed Gaussian state space models, J. R. Stat. Soc. Ser. B Stat. Methodol. 64 (2002) 827–836.
[48] B. Ristic, M.S. Arulampalam, N. Gordon, Beyond the Kalman Filter, Artech House, Boston, MA, 2004.
[49] S. Gabriel, R.W. Lau, C. Gabriel, The dielectric properties of biological tissues: III. Parametric models for the dielectric spectrum of tissues, Phys. Med. Biol. 41 (1996) 2271–2293.